ELSEVIER

Journal of Power Sources 77 (1999) 143–158

JOURNAL OF POWER SOURCES

Electronic-network modelling of rechargeable NiCd cells and its application to the design of battery management systems

H.J. Bergveld *, W.S. Kruijt, P.H.L. Notten

Philips Research Laboratories WAY51, Prof. Holstlaan 4, 5656AA Eindhoven, Netherlands

Received 16 July 1998; revised 10 November 1998; accepted 13 November 1998

Abstract

In the first part of this paper, the development of a simulation model for a sealed rechargeable NiCd cell is described. Based on the concept of this cell type, a mathematical description of the various physical and electrochemical processes occurring inside the cell can be given. Subsequently, these equations are introduced in the form of electronic components into an electronic-circuit simulator. This enables the user to simulate the most important cell characteristics like voltage, temperature and internal gas pressure simultaneously and coherently under a wide variety of charging, discharging and open-circuit conditions. The construction of the model enables the user to investigate the course of each of the various reactions taking place inside the cell. Moreover, the electrical and thermal interaction with the surrounding electronics attached to the cell and with other cells, e.g., in a battery pack, can also be simulated. In the second part of this paper, some examples of simulations of cell characteristics are presented. The results of the simulated phenomena show good qualitative agreement with measured cell characteristics. An understanding of phenomena such as charge efficiency, self-discharge and overdischarge is presented using the model. Simulation of battery behaviour in an electronic system enables a system designer to design the optimal Battery Management System around the battery. In the third part of this paper, an example of applying the model in an electronic system is given, i.e., a shaver. Also, simulations of several cells connected in series forming a battery or battery pack are described.

Keywords: Rechargeable NiCd cells; Rechargeable batteries; Modelling; Battery Management Systems; Simulation

1. Introduction

Nowadays, an increasing demand for portability of various electronic consumer products can be distinguished clearly. Therefore, the use of rechargeable batteries in these products is growing rapidly. Ultimately, the energy delivered by a rechargeable battery to a portable product originates from the electrical energy delivered by the mains. The conversion of energy from the mains to the load can be described as an energy chain, which is schematically drawn in Fig. 1. The links of the energy chain are a charger, a battery, a DC/DC converter and a load.

Electrical energy from the mains is fed to the battery through the charger during charging. In the charger, electromagnetic components like a transformer or an inductor are used, in which electrical energy from the mains is first transformed into magnetic energy and then back into electrical energy. In the battery, the electrical energy is stored in the form of chemical energy. During discharge of the battery, chemical energy is converted back into electrical energy. The DC/DC converter can be used for two reasons. First, the battery might deliver a voltage which is not suitable for operation of the load. Second, for efficiency reasons, each circuit part of the load should be operated from the lowest possible supply voltage, because a surplus in supply voltage is often dissipated in heat. In both cases, the DC/DC converter supplies the circuit parts in the load with the lowest possible supply voltage, irrespective of the battery voltage. In the DC/DC converter, an electromagnetic element, i.e., a storage inductor, is used, translating the electrical energy from the battery into magnetic energy and back into electrical energy again. In the load, the electrical energy from the DC/DC converter is converted into sound, vision, motion, EM radiation, etc.

* Corresponding author. Tel.: +31-40-2744244; Fax: +31-40-2744657; E-mail: bergveld@natlab.research.philips.com

0378-7753/99/$19.00
PII: S0378-7753(98)00188-8

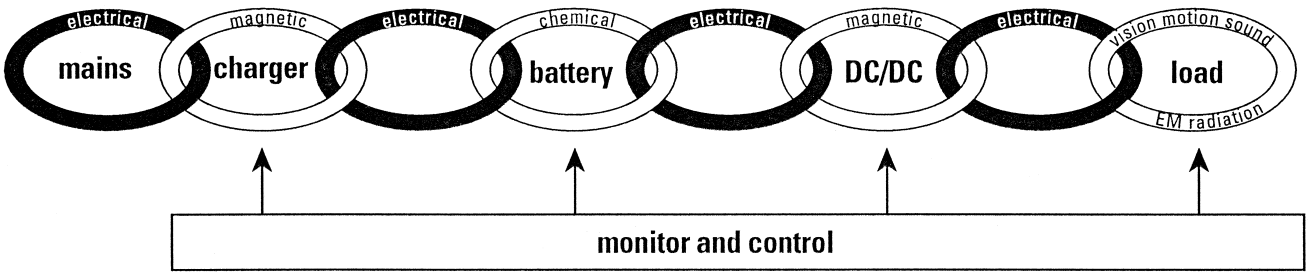

Fig. 1. The energy chain from mains to load for a portable product.

In order to make optimal use of the energy inside the battery, all conversions of energy in the energy chain should be well understood and made as efficient as possible, especially when miniaturization of the portable product is concerned. When the volume of a portable product decreases, the amount of dissipated power should decrease also, because a smaller volume will yield a higher temperature when the amount of dissipated power remains the same. In order to check all conversions of energy on efficiency, the operation of all links in the energy chain should be monitored and controlled. This is schematically shown in Fig. 1.

Simulation is a helpful tool to obtain optimal control algorithms for the links in the energy chain, since in depth knowledge of a wide range of disciplines is involved. Therefore, simulation models of all links in the energy chain are essential. For example, an approach for modelling transformers has been developed, using the physical parameters of the transformer (number of turns of the windings, core dimensions, material constants, etc.) and yielding an electronic circuit suitable for simulation in an electronic-circuit simulator [1]. In this paper, an approach to model rechargeable cells is described, applied to the well-known NiCd rechargeable cell. The model was implemented by using the electronic-circuit simulator PSTAR©, which is developed by and commonly used within Philips Electronics. Other circuit simulators, e.g., SPICE©, can also be used, as long as they allow the introduction of large sets of coupled nonlinear equations.

The optimal control algorithms resulting from simulation of the complete energy chain can be implemented in the form of optimal charging algorithms, State-of-Charge (SoC) algorithms, optimal supply voltages for the various system parts of the load, etc. Implementation of such algorithms form part of a so-called Battery Management System.

Modelling rechargeable batteries based on a mathematical description of the processes occurring inside the battery has often been reported in literature [2–13]. No use is made of an equivalent electronic circuit for these models which only describe the voltage characteristics of the battery. Moreover, none of these models considers the battery temperature and internal gas pressure development during operation of the battery and the interaction between these characteristics. In fact, in a sealed rechargeable battery system, the battery voltage, pressure and temperature are closely linked and their mutual influence is considerable. For example, both pressure and temperature influence the rate of the oxygen evolution and reduction reactions inside a battery. These reactions do not contribute to the accumulation of chemical energy inside the battery and hence, the battery pressure and temperature influence the charge and discharge efficiency.

Apart from purely mathematical models of rechargeable batteries, modelling rechargeable batteries using electronic equivalent circuits has also been described in literature [14–20]. Three approaches can be distinguished.

(i) The equivalent electronic circuit may consist of linear passive elements, i.e., resistances, capacitances and inductances, to account for the impedance of batteries [14–17]. However, due to the complex non-linear behaviour of batteries, these models generally fail to describe the most important battery characteristics.

(ii) The equivalent electronic circuit may consist of linear passive elements in combination with voltage sources describing the battery behaviour using look-up tables [18,19]. With this approach the simulated battery characteristics can only be realized through interpolation of the tabulated data. Moreover, the accuracy of this type of model depends strongly on the amount and reliability of the tabulated data.

(iii) An equivalent electronic-circuit model of a rechargeable NiCd cell based on non-linear passive and active elements configured around a PIN-diode model has been reported [20]. Again, in this model the influence of cell pressure and temperature on the behaviour of the cell is not taken into account. Also, many parameters in the model do not have any electrochemical significance.

In the approach of modelling rechargeable cells described in this paper, a mathematical model of the rechargeable cell is derived first. This model is based on the charge transfer kinetics and mass transport limitations of the various reactions and physical processes occurring during (over)charging, resting and (over)discharging. Then, for each process the mathematical equations are clustered and these clusters are represented by linear and non-linear

equivalent electronic-circuit elements, which are combined in an electronic network. In this electronic network, three domains can be distinguished, i.e., the electrical domain, the chemical domain and the thermal domain. These domains are coupled, modelling the mutual influence of the cell voltage, pressure and temperature characteristics, respectively. The pressure is derived from the molar amount of oxygen in this case, which is calculated in the chemical domain.

The advantage of the approach described in this paper is the possibility to simulate the cell or a combination of cells, i.e., a battery, in an electronic environment, using an electronic-circuit simulator, taking the battery voltage, pressure and temperature and their mutual influence into account [21–24]. Because the model is based on an electrochemical and physical battery theory, the origin of specific battery behaviour can be examined by studying both the local currents and voltages in the equivalent electronic network. As an advantage, all parameters in the model have an electrochemical significance and can therefore be determined from experiments or literature.

In Section 2 some general information about the construction and operation of sealed rechargeable NiCd cells is given. Section 3 describes their equivalent electronic network. Some simulation results of a NiCd cell are described in Section 4. An understanding of battery phenomena such as charge efficiency, self-discharge and overdischarge is presented using the model. In Section 5, some simulations are described giving examples of the interaction between the battery and its electronic and thermal environment. Finally, conclusions are drawn in Section 6.

2. Basic operational mechanism of sealed rechargeable NiCd cells

The rechargeable NiCd cell is still commonly used nowadays. It is relatively cheap, robust, and it has the ability to supply a large current, which makes it the obvious choice, e.g., for power tools. It has a cell voltage of around 1.3 V and a capacity ranging roughly from 600 to 1000 mAh in standard AA size, depending on the type and manufacturer. The construction of a NiCd cell depends on its application area, e.g., large-capacity cell or high-power drain cell. In all cases, the cell is sealed, yielding a closed system. A vent is present to allow the cell to vent during extreme pressure buildup.

A schematic representation of a mature construction of a sealed rechargeable NiCd cell is given in Fig. 2. This construction was chosen as the basis for deriving the cell model in this paper. The three basic elements in Fig. 2 are: the positive nickel electrode, the negative cadmium electrode, and a concentrated KOH electrolyte solution. To prevent electrical contact between the positive and negative electrodes, both electrodes are separated by a thin porous layer of insulating material, the separator.

2.1. Main storage reactions taking place during charging and discharging

The electrochemical storage reactions are given in the region denoted as *storage capacity* in Fig. 2. The arrows pointing upwards denote the charging reactions, whereas the arrows pointing downwards denote the discharging

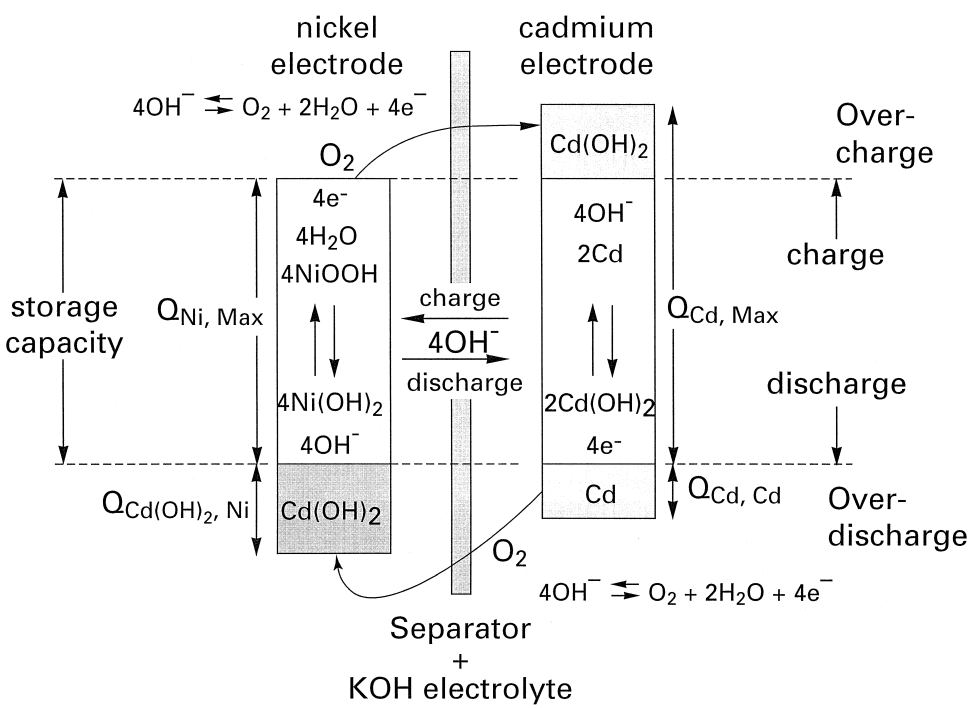

Fig. 2. Schematic representation of a sealed rechargeable NiCd cell.

reactions. During charging, at the nickel electrode $Ni(OH)_2$ is oxidised to NiOOH. At the same time, $Cd(OH)_2$ is reduced to metallic Cd at the cadmium electrode. During discharging, the reverse reactions take place. Current flow inside the cell is supported by electrons inside the electrodes and by OH^- ions inside the electrolyte. Externally, the current flows through the charger and/or load.

2.2. Side reactions taking place during overcharging and overdischarging

Besides the main storage reactions, electrochemical side reactions also take place, especially during overcharging and overdischarging. Overcharging means continuing charging the cell when it is full, whereas overdischarging means continuing discharging the cell when the cell voltage reaches the value of 0 V. The latter situation occurs, for example, in batteries or battery packs with several cells in series, as will be explained in Section 5. These side reactions include oxygen evolution and reduction reactions, denoted in Fig. 2 by the curved arrows, and a cadmium side reaction at the nickel electrode, denoted by the grey area $Cd(OH)_2$ at the nickel electrode in Fig. 2. All grey areas in Fig. 2 symbolize the excess material added to the NiCd cell to protect it from too high pressure buildup inside the cell during overcharging and overdischarging. The way in which this is achieved is discussed below.

2.2.1. Overcharging

An overcharge reserve of excess $Cd(OH)_2$ is added to the cadmium electrode to prevent too high pressure buildup during overcharging. Hence, the nickel electrode is the capacity determining electrode, which is reflected in $Q_{Ni,Max}$ being smaller than $Q_{Cd,Max}$ in Fig. 2. As a result, during the charge process the nickel electrode will run out of $Ni(OH)_2$ before the cadmium electrode will run out of $Cd(OH)_2$. A different oxidation reaction has to occur at the nickel electrode, which will start to produce oxygen, whereas metallic Cd is still formed at the cadmium electrode because of the excess $Cd(OH)_2$. Evolution of oxygen at the nickel electrode takes place by oxidizing OH^- ions into oxygen and water molecules. When the oxygen pressure increases, oxygen molecules can diffuse to the cadmium electrode and the oxygen reduction reaction starts to compete with the Cd forming reaction. The oxygen molecules can be reduced to OH^- ions. Especially, the reduction of oxygen at the cadmium electrode generates a lot of heat, which leads to a rise in temperature, as will be described in Section 4.

2.2.2. Overdischarging

An overdischarge reserve of excess $Cd(OH)_2$, generally denoted as depolarizer, is added to the nickel electrode in the amount $Q_{Cd(OH)_2,Ni}$ as indicated in Fig. 2. Additionally, some metallic cadmium is added to the cadmium electrode in an amount $Q_{Cd,Cd}$ smaller than $Q_{Cd(OH)_2,Ni}$. This is done to enforce a similar oxygen evolution and reduction process as occurring during overcharging. In this way, the evolution of hydrogen gas at the nickel electrode is prevented and a hydrogen evolution/oxidation cycle is avoided [25]. Because of the excess of metallic Cd in the cadmium electrode, the nickel electrode will run out of NiOOH before the cadmium electrode will run out of metallic Cd. At this moment, the excess $Cd(OH)_2$ at the nickel electrode will be reduced to metallic Cd and the oxidation reaction the other way around still occurs at the cadmium electrode. When discharging proceeds to the stage where the cadmium electrode runs out of metallic Cd, the cadmium electrode will start to produce oxygen gas, leading to a rise in oxygen pressure. When the oxygen pressure increases, the oxygen reduction reaction starts to compete with the $Cd(OH)_2$ reduction reaction at the nickel electrode and a similar situation as during overcharging occurs.

For each electrochemical reaction, a standard electrode potential can be defined vs. a reference electrode. For the nickel and cadmium electrode reactions as indicated in Fig. 2, the standard electrode potentials at 298 K vs. SHE (Standard Hydrogen Electrode) are 0.520 V and -0.808 V, respectively [26]. Assuming that the state of the nickel and cadmium electrode reactions only causes a relatively low deviation of the actual electrode potentials from the standard electrode potentials, the standard potential difference between the two electrodes leads to a theoretical open circuit voltage of 1.328 V for the complete NiCd cell. For the oxygen reaction, the standard electrode potential vs. SHE at 298 K is 0.401 V [26].

3. An equivalent electronic-network model of a NiCd cell

As was explained in the Section 1, the most important electrochemical and physical processes occurring in a rechargeable NiCd cell can be described by a set of mathematical equations. For each of these processes an equivalent electronic circuit consisting of one or more elements can be designated, which behaves according to the corresponding mathematical equations. Hereby, use is made of the analogy in energy and power definitions in the several domains, i.e., the electrical domain, the chemical domain and the temperature domain [27]. The analogy between the electrical, chemical and thermal domains is made clear in Table 1. In each domain, an effort variable e and a flow variable f can be defined, which are given in the first two rows of Table 1, e.g., in the electrical domain, the effort is voltage and the flow is current. The displacement variable is defined as the integral of the flow variable and is shown in the fourth row of Table 1. Note that the choice of heat as the displacement variable in the thermal domain leads to a definition of ‘power’ and ‘energy’ which is not physical as can be seen from the unit. Using

Table 1
Analogy between the electrical, chemical and thermal domains

Electrical domain			Chemical domain			Thermal domain		
Quantity	Symbol	Unit	Quantity	Symbol	Unit	Quantity	Symbol	Unit
Voltage	V	V	Chemical potential	μ	J/mol	Temperature	T	K
Current	I	A	Chemical flow	J_{ch}	mol/s	Heat flow	J_{th}	W
Electrical power	$P_{el} = VI$	W	Chemical power	$P_{ch} = \mu J_{ch}$	W	'Thermal power'	$P_{th} = TJ_{th}$	WK
Charge	$Q = It$	C	Molar amount	$m = J_{ch} t$	mol	Heat	$Q_{th} = J_{th} t$	J
Electrical energy	$E_{el} = P_{el} t$	J	Chemical energy	$E_{ch} = P_{ch} t$	J	'Thermal energy'	$E_{th} = P_{th} t$	JK
Electrical capacitance	$C_{el} = Q/V$	F	Chemical capacitance	$C_{ch} = m/\mu$	mol^2/J	Thermal capacitance	$C_{th} = Q_{th}/T$	J/K
Electrical resistance	$R_{el} = V/I$	Ω	Chemical resistance	$R_{ch} = \mu/J_{ch}$	Js/mol^2	Thermal resistance	$R_{th} = T/J_{th}$	K/W

entropy as displacement variable would solve this problem. However, for practical reasons the use of heat as displacement variable in the thermal domain is generally accepted [27].

Domains can be linked by an ideal transformer, representing the energy exchange between the domains. For an ideal transformer linking domains 1 and 2, it holds that $e_2 = N * e_1$ and $f_1 = N * f_2$, where N denotes the transformer coefficient, which has a dimension dependent on the dimensions of e and f of the domains it links. By combining the equivalent electronic circuits of all important processes in an electronic network, a cell model can be created, in which the individual processes as well as the relation between the processes can be modelled.

The complete equivalent electronic-network model for a sealed rechargeable NiCd cell based on the schematic representation shown in Fig. 2 is shown in Fig. 3. Fig. 3a represents the equivalence of the electrochemical behaviour and Fig. 3b of the thermal behaviour. In Fig. 3a, the nickel electrode model is shown on the left side, whereas the cadmium electrode model is shown on the right side. The electrodes are modelled by a series resistance R, representing the electronic conductivity of the electrode material, in series with a parallel connection of several reaction paths and a capacitance C^{dl}, representing the double-layer capacitance. This double-layer capacitance is a result of the charge separation effect taking place at the electrode surface in the electrolyte. The electrodes are separated by a resistance R_e, modelling the ionic conductivity of the electrolyte and separator. In the part of the equivalent electronic network, representing the nickel electrode, three reaction paths in parallel can be distinguished, which denote from top to bottom: (i) the nickel storage reaction, (ii) the oxygen side reaction, and (iii) the cadmium side reaction. In the part of the equivalent electronic network, representing the cadmium electrode, two reaction paths in parallel can be distinguished, which denote from top to bottom: (i) the cadmium storage reaction and (ii) the oxygen side reaction.

Two domains can be distinguished in Fig. 3a, i.e., the electrical and the chemical domain. Energy storage in the electrical domain is modelled by capacitances C^{dl}, while energy storage in the chemical domain is modelled by non-linear capacitances C_i, where i denotes the reacting species. The coupling between the electrical and chemical domain is represented by ideal transformers, which represent energy transfer between the electrical and chemical domain through an electrochemical reaction. Each reaction path j is modelled as an ideal transformer in series with two antiparallel diodes D_j, where one diode represents the oxidation reaction and the other represents the reversed reduction reaction. The voltage across each transformer equals the so-called equilibrium potential V_j^{eq} of the corresponding redox reaction, whereas the voltage across each pair of antiparallel diodes represents the so-called overpotential for the corresponding redox reaction. This overpotential can be seen as the driving force for the redox reaction and it has a non-zero value under non-equilibrium conditions, i.e., when current flows through a reaction path. In this case, the electrode potential equals the sum of the equilibrium and over potential.

The network shown in Fig. 3b represents the thermal domain and is used to calculate the cell temperature (see also Table 1). Heat production inside the cell originates from the various reactions and heat dissipation in ohmic resistances. These heat producing sources are represented by heat flow sources J_{th_k}, where the index k indicates the origin of the heat flow. The net heat flow of heat production inside the cell and heat flow to the environment, as represented by the thermal resistance R_{th}, is integrated in the cell thermal capacitance C_{cell}. The amount of charge on this capacitance represents the amount of heat in the cell and the voltage across this capacitance represents the internal cell temperature T_{cell} using the analogy of Table 1. C_{amb} represents the thermal capacitance of the environment, where the voltage across this capacitance corresponds to the ambient temperature T_{amb}. A temperature difference between the cell and its environment will result in a heat flow through thermal resistance R_{th}, which is inversely proportional to the surface area of the cell. Also, the value of this resistance depends on the material of the cell.

Considering an AA size NiCd cell, the value of the resistances R_{Ni} and R_{Cd} are fixed at 2 mΩ, including the contact resistance between the metallic current collector and the electroactive species and the resistance of the

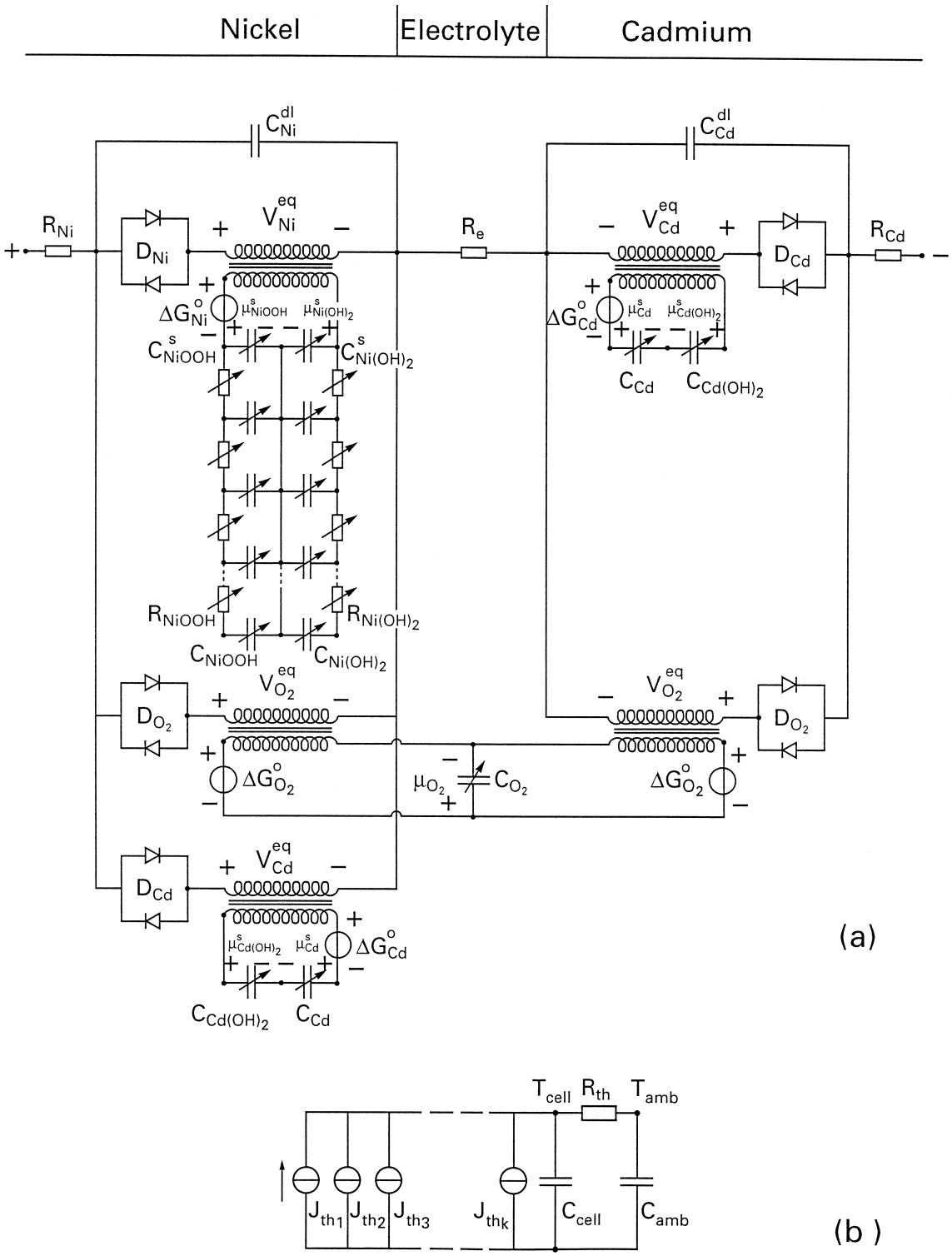

Fig. 3. Equivalent electronic-network model of a rechargeable NiCd cell based on the schematic representation of Fig. 2.

electroactive species itself [28]. The ionic conductivity of the electrolyte is assumed to be constant during cell operation, leading to a constant value of the resistance R_e representing the electrolyte. Again considering an AA size NiCd cell, the value of the electrolyte resistance is fixed at 10 mΩ, which is in the range of reported values for NiCd cells. Both values of the double-layer capacitances are based on the value of the double-layer capacitance per unit area of 0.2 F/m^2 [29] and typical morphology of both porous electrodes. The double-layer capacitance of the cadmium electrode is larger than that of the nickel electrode, because its surface area is larger, due to the excess

Cd and $Cd(OH)_2$ (see Fig. 2). In the present model, a value of 2.4 F is assumed for the double-layer capacitance of the nickel electrode C_{Ni}^{dl}, whereas a value of 4.7 F is assumed for C_{Cd}^{dl}. A value of 14 J/K for C_{cell} and a value of 25 K/W for R_{th} is estimated for the AA size NiCd cell in this paper. If the value of C_{amb} is taken very high, the temperature outside the cell will be more or less fixed at the ambient temperature. Even if the cell heats up considerably, resulting in a high cell temperature which is modelled by a large voltage across capacitance C_{cell}, the ambient temperature modelled by the voltage across capacitance C_{amb} will hardly change. An example of a more complex thermal model of the cell environment will be given in Section 5. The parameter values related to the construction of the AA size NiCd cell considered in the simulations in later sections are summarized in the upper part of Table 2.

In general, for each reacting species i taking place in a reaction in the chemical domain, a chemical potential can be defined (see also Table 1). In an electrochemical reaction, apart from non-charged reacting species, charged reacting species, i.e., electrons and ions, are involved. In that case, the term electrochemical potential is used. The general expression for an electrochemical potential $\overline{\mu}$ of a reacting species i in a reaction taking place at the electrode surface s is given by Eq. (1) [29].

$$\overline{\mu}_i = \mu_i^0 + RT\ln\left(\frac{a_i^s}{a_{i,ref}}\right) + zF\phi \quad (1)$$

In Eq. (1), μ_i^0 denotes the standard chemical potential of reacting species i (in J/mol), R denotes the gas constant ($R = 8.314$ J/mol K), T the absolute temperature (in K), a_i^s the surface activity of reacting species i (in mol/m^3), $a_{i,ref}$ the activity of reacting species i in the reference state, z the charge number of reacting species i, F the Faraday constant ($F = 96485$ C/mol) and ϕ the electrostatic potential associated with reacting species i

Table 2
Most important parameter values of considered rechargeable NiCd cell model used in simulations

Parameter	Value	Unit	Description
Construction related parameters (AA size 600 mAh NiCd cell)			
R_{Ni}	2	mΩ	Ohmic resistance nickel electrode
R_{Cd}	2	mΩ	Ohmic resistance cadmium electrode
R_{el}	10	mΩ	Ohmic resistance 8 M KOH electrolyte
C_{Ni}^{dl}	2.4	F	Double-layer capacitance nickel electrode
C_{Cd}^{dl}	4.7	F	Double-layer capacitance cadmium electrode
A_{Ni}	11.8	m^2	Effective surface area nickel electrode
A_{Cd}	23.3	m^2	Effective surface area cadmium electrode
$Q_{Ni,Max}$	3060	C	Maximum storage capacity nickel electrode (see Fig. 2)
$Q_{Cd,Max}$	5000	C	Maximum storage capacity cadmium electrode (see Fig. 2)
$Q_{Cd(OH)_2,Ni}$	1000	C	Overdischarge reserve of $Cd(OH)_2$ in nickel electrode (see Fig. 2)
$Q_{Cd,Cd}$	800	C	Overdischarge reserve of Cd in cadmium electrode (see Fig. 2)
V_g	1.5×10^{-6}	m^3	Free gas volume inside the cell
Electrochemistry-related parameters			
ΔG_{Ni}^o	5.0×10^4	J/mol	Standard free energy change for nickel reaction at 298 K
ΔG_{Cd}^o	-1.6×10^5	J/mol	Standard free energy change for cadmium reaction at 298 K
$\Delta G_{O_2}^o$	1.5×10^5	J/mol	Standard free energy change for oxygen reaction at 298 K
n_{Ni}	1	–	Principal number of electrons involved in nickel reaction
n_{Cd}	2	–	Principal number of electrons involved in cadmium reaction
n_{O_2}	4	–	Principal number of electrons involved in oxygen reaction
α_j	0.5	–	Charge transfer coefficient for all reactions
I_{Ni}^o	0.036×10^3	A	Exchange current nickel reaction at 50% SoC
I_{Cd}^o	2.3×10^3	A	Exchange current cadmium reaction at 50% SoC
$(I_{O_2}^o)_{Ni}^{ox}$	117.6×10^{-9}	A	Exchange current O_2 evolution reaction at nickel electrode at 10^5 Pa partial oxygen pressure
$(I_{O_2}^o)_{Cd}^{ox}$	23×10^{-3}	A	Exchange current O_2 evolution reaction at cadmium electrode at 10^5 Pa partial oxygen pressure
$(I_{O_2}^o)_{Ni}^{red}$	0.5×10^{-3}	A	Exchange current O_2 reduction reaction at nickel electrode at 10^5 Pa partial oxygen pressure
$(I_{O_2}^o)_{Cd}^{red}$	2.3×10^{-3}	A	Exchange current O_2 reduction reaction at cadmium electrode at 10^5 Pa partial oxygen pressure
$D_{H^+}^o$	5×10^{-14}	m^2/s	Diffusion coefficient of H^+ ions at 298 K
$D_{OH^-}^o$	5×10^{-10}	m^2/s	Diffusion coefficient of OH^- ions at 298 K
$D_{O_2}^o$	5×10^{-10}	m^2/s	Diffusion coefficient of O_2 molecules at 298 K
d_{OH^-}	1×10^{-6}	m	Diffusion layer thickness of OH^- ions for cadmium reaction
d_{O_2}	3×10^{-7}	m	Diffusion layer thickness of O_2 molecules

(in V). Note that the third term in Eq. (1) is zero for non-charged reacting species. The activity a_i^s of species i is assumed linearly proportional to its concentration and to its molar amount m_i through an activity coefficient, where the volume in which the species i is present is assumed constant. Although in concentrated solutions, the activity coefficient is dependent on the concentration, it is assumed constant in the present model [30].

All species i with a varying value of a_i^s in the course of the reaction are represented by non-linear capacitances, the voltage across which corresponds to the chemical potential μ_i and the charge on which corresponds to the molar amount m_i of species i (see also Table 1). For each non-linear capacitance C_i, the relation between μ_i and m_i is given by Eq. (1) using the activity coefficient . Note that the signs of the chemical potentials are opposite for species at the opposite side of the arrow in the reaction equation, see also the reaction equations in Fig. 2. In the present model, as a simplification, the activities a_i^s of reacting species water and OH^- ions, hence, their concentrations, are assumed to be constant and uniform across the cell. Therefore, the second term in Eq. (1) is taken constant for both species. However, the model can easily be adapted to include for instance a variable surface activity $a_{OH^-}^s$ of OH^- ions, by including a non-linear capacitance C_{OH^-} in series with the other non-linear capacitances for all reactions where OH^- ions are involved. Also, the activities a_i^s and $a_{i,ref}$ of an electron are unity by definition. Therefore, the second term in Eq. (1) is zero for electrons. In the chemical domain in Fig. 3, for each reaction j, all constant terms of the electrochemical potentials of the reacting species in an electrochemical reaction are combined in a voltage source ΔG_j^o, which represents the standard free energy change for reaction j. Note that the value of ΔG_j^o is dependent on temperature.

For the nickel reaction, the molar amount of NiOOH, which is formed during charging, is directly related to the SoC. For the oxygen reaction, the net molar amount of oxygen is related to the oxygen pressure through the general gas law $PV_g = mRT$, with P as the oxygen pressure, V_g as the free gas volume inside the cell and m as the number of moles of oxygen present inside the free gas volume. As explained in Section 2, when oxygen is produced at one electrode, it can be consumed at the other electrode. This can be seen in Fig. 3a by the coupling of the non-linear capacitance C_{O_2} to both electrodes by means of ideal transformers. The chemical flow of oxygen evolution is into C_{O_2}, whereas the chemical flow of oxygen reduction is out of C_{O_2}. The net chemical flow of oxygen is integrated in C_{O_2}, yielding the net molar amount of oxygen.

In equilibrium, the net sum of the electrochemical potentials of all species i taking place in an electrochemical reaction is zero [30]. This can be seen in Fig. 3a for each reaction j by applying Kirchhoff's voltage law to the loop consisting of non-linear capacitances C_i, voltage source ΔG_j^o and the secondary coil of the ideal transformer in the chemical domain for each electrochemical reaction. Also, in equilibrium, the surface activity a_i^s is equal to the bulk activity a_i^b of species i, i.e., there is no concentration gradient of species i. For each electrochemical reaction, electrons can be found at one side of the arrow of the reaction equation, whereas OH^- ions can be found at the other side (see also Fig. 2). For electrons, the electrostatic potential ϕ in Eq. (1) represents the electrostatic electrode potential ϕ^s, whereas for OH^- ions, the electrostatic potential ϕ in Eq. (1) represents the electrostatic electrolyte potential ϕ^l. As a result, a voltage $zF(\phi^s - \phi^l)$ is present across the secondary coil of the transformer in the chemical domain. The transformer coefficient is $1/n_jF$, with n_j the number of electrons involved in the electrochemical reaction j. This leads to the following equation for the equilibrium potential of reaction j, V_j^{eq}:

$$V_j^{eq} = \frac{\Delta G_j^o}{n_j F} + \frac{RT}{n_j F}\ln\frac{\prod_p a_{p,ox}^s}{\prod_q a_{q,red}^s}$$

$$= V_j^o + \frac{RT}{n_j F}\ln\frac{\prod_p a_{p,ox}^s}{\prod_q a_{q,red}^s} = \phi^s - \phi^l \qquad (2)$$

In Eq. (2), V_j^o denotes the standard electrode potential of reaction j (in V) (see Section 2). The numerator of the ln term in Eq. (2) equals the product of all surface activities a_p^s of the oxidising species p in an electrochemical reaction, whereas the denominator of the ln term in Eq. (2) equals the product of all surface activities a_q^s of the reducing species q in this reaction. The difference $\phi^s - \phi^l$ equals the potential of the electrode where reaction j takes place. The values of ΔG_j^o and n_j for reaction j used in the simulations in this paper are summarized in Table 2.

In a non-equilibrium situation, the net current flowing through the antiparallel diodes D_j for each redox reaction j equals the difference between the currents flowing through the oxidation (I_{ox_j}) and the reduction reaction diode (I_{red_j}). The relation between this net current flowing through a reaction path and the overpotential η_j across the anti-parallel diodes D_j is given in Eq. (3), which is known as the Butler–Volmer equation describing the reaction kinetics [31]. This equation is used for the anti-parallel diodes D_j in Fig. 3a.

$$I_j^{kin} = I_{ox_j} - I_{red_j} = I_j^o\left(a_i^b\right)e^{\frac{\alpha_j n_j F\eta_j}{RT}} - I_j^o\left(a_i^b\right)e^{\frac{-(1-\alpha_j)n_j F\eta_j}{RT}} \qquad (3)$$

In Eq. (3), the diode-like current–voltage relation for the reaction currents I_{ox_j} and I_{red_j} can be clearly recognized. The terms $RT/\alpha_j n_j F$ and $RT/(1-\alpha_j)n_j F$ resemble the well-known thermal voltage kT/q in semiconductor physics, where α_j denotes the dimensionless charge transfer coefficient of reaction j, with $0 < \alpha_j < 1$. The term

$I_j^o(a_i^b)$ denotes the exchange current of reaction j, which is a function of the bulk activities a_i^b of the reacting species i [23,24]. In a general form, the dependency of the exchange current of reaction j on the bulk activities of the oxidising and reducing species in the reaction is given by [31]:

$$I_j^o = n_j F A_j k_j \left(\prod_p a_{p,ox}^b \right)^{\alpha_j} \left(\prod_q a_{q,red}^b \right)^{1-\alpha_j} \quad (4)$$

where A_j is the electrode surface area at which reaction j takes place (in m^2) and k_j is the standard rate constant of reaction j. The exchange current of a redox reaction determines the kinetics of the reaction, i.e., a redox reaction with a low value of the exchange current will proceed relatively slowly, whereas a high value corresponds with a relatively fast reaction. Note that the value of the exchange current for each redox reaction will change when the reaction proceeds, because the bulk activities of some reacting species will change. The values of α_j, n_j and I_j^o for chosen values of a_i^b used in the simulations in this paper are summarized in Table 2. Note that for the oxygen reaction, different values of the exchange current are used for the oxidation and reduction reactions at different electrodes [24].

Apart from the kinetics of a redox reaction, which determines the reaction rate through the value of the exchange current, the supply and removal of the reacting species to and from the surface of the electrodes can also determine the rate of a reaction. We assume that mass transport of reacting species inside the cell mainly takes place through diffusion. In general, diffusion limitation of a reaction leads to concentration profiles of the reacting species and hence to differences between the bulk activities a_i^b and the surface activities a_i^s. This leads to a deviation of the equilibrium potential given in Eq. (2), for which $a_i^s = a_i^b$, which can be expressed by an apparent equilibrium potential $V_i^{eq\prime} = V_i^{eq} + \eta_d$, where η_d represents the diffusion over potential. Diffusion limitation plays a role in all electrochemical reactions concerned in the model presented in this paper. In the present model for the nickel reaction, the diffusion of H^+ ions in the solid-state nickel electrode is considered, for the cadmium reaction the diffusion of OH^- ions in the electrolyte is considered and for the oxygen reaction the diffusion of O_2 molecules in the electrolyte is considered.

In the nickel electrode, during charging, $Ni(OH)_2$ is oxidised into NiOOH, and a H^+ ion and an electron are released. The H^+ ion diffuses through the nickel electrode to the electrode surface by 'hopping' from one NiOOH site to the other. Diffusion limitation of H^+ ions leads to a concentration profile of both the NiOOH and $Ni(OH)_2$ species in the nickel electrode, where the concentration profile of NiOOH is the reverse of that of $Ni(OH)_2$. Hence, the apparent equilibrium potential $V_{Ni}^{eq\prime}$ is now valid for the Ni reaction. The RC network depicted in Fig. 3a is used to calculate the surface activity a_i^s and the concentration profiles for both NiOOH and $Ni(OH)_2$. The electrode is therefore subdivided into x compartments, with each capacitance C_x representing the molar amount of NiOOH and $Ni(OH)_2$ in compartment x, respectively. The value of the resistances depends on the value of the diffusion coefficient for protons D_{H^+} in the nickel electrode. This diffusion constant is temperature-dependent.

For the cadmium and oxygen reaction, a simpler approach was used in the present model to include the influence on the electrode potential of the diffusion of OH^- ions and O_2 molecules, respectively. In both cases stationary diffusion with a linear concentration gradient across a thin diffusion layer with fixed thickness d was assumed. This assumption is allowed when the time to build the diffusion layer is much smaller than a typical charge–discharge time of the cell. In the case of stationary diffusion, the diffusion current I_i^{dif} for diffusing species i can be calculated from Ficks first law, yielding [29,31]:

$$I_i^{dif} = \frac{nFA_i D_i a_i^b}{d_i}. \quad (5)$$

In Eq. (5), A_i denotes the area through which the species i diffuses (in m^2), D_i the temperature-dependent diffusion coefficient of the diffusing species i and d_i the diffusion layer thickness (in m). Assuming a combined kinetic-diffusion controlled reaction j involving the diffusing species i, the overall reaction current I_j can be found from [31]:

$$I_j = \frac{I_j^{kin} I_i^{dif}}{I_j^{kin} + I_i^{dif}} \quad (6)$$

where I_j^{kin} is found from Eq. (2). Using Eq. (6) for the diode D_j for the cadmium and oxygen reactions, the diffusion limitation of OH^- ions and O_2 molecules leads to the diffusion potential η_d being present across the diodes D_j. As an extension to the present model, non-linear capacitances C_{OH^-} could be added to the model of Fig. 3 describing the surface activities of OH^- ions. Similar RC networks as for the $Ni(OH)_2$ and NiOOH species can then be used to calculate the OH^- concentration profile throughout the electrolyte. The values of the diffusion coefficients D_i and diffusion layer thicknesses d_i used in the simulations in this paper can be found in Table 2.

During current flow, in each electrode the current divides itself over the available reaction paths. Which reactions will occur depends on the value of the equilibrium potential of each reaction and the rate with which each reaction can take place. In principle, the redox reaction j with the lowest value of the equilibrium potential V_j^{eq} will thermodynamically be more favourable than a redox reaction with a higher value of V_j^{eq}. Applying Kirchhoff's voltage law to two reaction paths in parallel, this means that the thermodynamically favourable reaction has a higher overpotential η. However, as can be seen from Eq. (3), this does not necessarily mean that this reaction will actually take place, because the reaction rate might be too

low. This low rate might be caused by either a low exchange current or diffusion limitation.

4. Simulation results

In this section some simulation results performed with the model of a single AA size 600 mAh NiCd cell with the parameter values listed in Table 2 are described. The model is based on the schematic description shown in Fig. 2. Fig. 4 shows the simulated voltage, oxygen pressure and temperature development as a function of the SoC during charging with a current of 600 mA at an ambient temperature of 25°C. Fig. 5 shows similar curves, measured under the same conditions as assumed in the simulations, with an AA size 600 mAh NiCd cell for which the parameter values in Table 2 were derived.

The simulated curves are in good qualitative agreement with the measured curves. When the cell is not yet fully charged, the voltage rises gradually, whereas the pressure and temperature remain relatively constant. When the cell SoC approaches 100% and charging is continued, the voltage, and consequently the oxygen pressure, starts to rise more steeply. Especially, from the moment when the oxygen pressure starts to level off, the temperature starts to rise. Because of the temperature rise, the cell voltage will drop. This phenomenon is commonly known as the $-\Delta V$ effect, which is often used in fast chargers as an End-of-Charge criterion. The quantitative differences between Figs. 4 and 5 are largely due to the fact that many parameters in the cell model are not precisely known at present, but they have been chosen in the range encountered in the open literature. However, all parameters in the model have an electrochemical or physical meaning and research continues in order to measure the exact value of some of these parameters in order to obtain a better quantitative agreement between simulations and measurements.

The simulated curves shown in Fig. 4 can be understood from the equivalent electronic network model of the

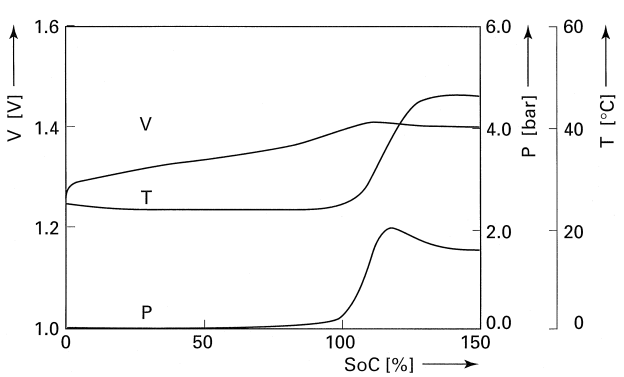

Fig. 4. Simulated voltage (V), oxygen pressure (P) and temperature (T) curves as a function of State-of-Charge (SoC) during charging at 25°C with a current of 600 mA for an AA size 600 mA h rechargeable NiCd cell.

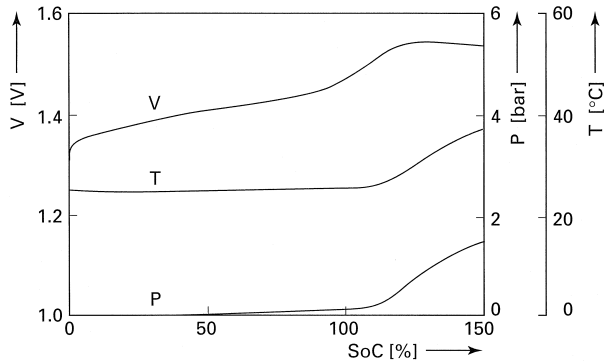

Fig. 5. Measured voltage (V), oxygen pressure (P) and temperature (T) curves as a function of State-of-Charge (SoC) during charging at 25°C with a current of 600 mA for an AA size 600 mAh rechargeable NiCd cell.

NiCd cell in Fig. 3. During charging, the current will flow from left (positive terminal) to right (negative terminal). From 0% SoC to about 90% SoC, the current will flow through the nickel reaction path (D_{Ni} and transformer) and chemical energy will be stored in the non-linear capacitances in the RC network of the nickel electrode under the assumed conditions. The molar amount in capacitances C_{NiOOH} will increase, whereas the molar amount in capacitances $C_{Ni(OH)_2}$ will decrease. In the cadmium electrode, the current will flow through the cadmium reaction path (D_{Cd} and transformer) and the molar amount in capacitance C_{Cd} will increase, whereas the molar amount in capacitance $C_{Cd(OH)_2}$ will decrease. Although the oxygen reaction path in the nickel electrode has a higher overpotential than the nickel reaction, a negligible amount of oxygen will be formed at the nickel electrode at the beginning of charging. This is caused by the relatively low rate of the oxygen evolution reaction, which results in a low exchange current $I^o_{O_2}$ in Eq. (3) for oxygen reaction diodes D_{O_2}. A negligible amount of current will flow through the Cd reaction path at the nickel electrode, because under normal charging conditions only $Cd(OH)_2$ is present and no metallic Cd, which could be oxidized into $Cd(OH)_2$. A negligible reduction current will flow through the oxygen reaction path at the cadmium electrode, because there is a negligible amount of oxygen gas present during the first stages of charging.

When charging is continued, the decrease in molar amount of $Ni(OH)_2$ will lead to a lower exchange current I^o_{Ni} for the nickel reaction through Eq. (4) and hence, a higher overpotential η_{Ni} for a constant current I (see Eq. (3)). At the same time, the apparent equilibrium potential $V^{eq\prime}_{Ni}$ rises according to Eq. (2), where the surface activities are not equal to the bulk activities. The increase of η_{Ni} and $V^{eq\prime}_{Ni}$ results in a steep rise of the cell voltage. Consequently, the overpotential of the oxygen reaction also rises, as can be understood from applying Kirchhoff's voltage law to the parallel combination of the nickel and oxygen reaction paths. An increase in overpotential for the oxygen

reaction eventually allows some oxygen to be formed. This will lead to an increase in exchange current $I^{o}_{O_2}$ for the oxygen reaction and the oxygen reaction will gradually take over from the nickel reaction.

As a result of the current flowing through the oxygen reaction path at the nickel electrode, the molar amount of oxygen in capacitance C_{O_2} increases, which leads to an increase in internal oxygen pressure. Owing to the available oxygen, current may now also start to flow through the oxygen reaction path at the cadmium electrode, which represents the reduction of oxygen. As a result, in the chemical domain the oxygen reduction flow will have the opposite direction of the oxygen evolution flow induced at the nickel electrode and the internal oxygen pressure will level off. Moreover, in the simulation of Fig. 4, the pressure even drops slightly, because the supposed temperature dependence of the oxygen reduction reaction is somewhat high in comparison to the experimental results. Therefore, at high temperatures, the reduction rate becomes higher than the evolution rate. Determination of the exact temperature dependence of these parameters needs further investigation.

As was explained in Section 2, there is a large difference between the standard electrode potentials V^{o} of the cadmium and oxygen reaction, and hence between the equilibrium potentials V^{eq}_{Cd} and $V^{eq}_{O_2}$. Applying Kirchhoff's voltage law to the parallel connection of the cadmium and oxygen reaction path at the cadmium electrode reveals that there will be a large overpotential η across the diodes D_{O_2} during overcharging. When a reaction takes place with a high overpotential, it will generate a relatively large heat flow J_{th_k}, because heat flow generated by a reaction is proportional to $I_{reaction}\eta_{reaction}$ [32]. Hence, the current source J_{th_k} in Fig. 3b representing the oxygen reduction at the cadmium electrode will attain a large value. As a result, the cell temperature will start to rise steeply in this overcharge region. Because the standard electrode potentials V^{o} and the overpotentials η have a negative temperature coefficient, the cell voltage will decrease because of the rising temperature, yielding the $-\Delta V$ effect.

The division of current between the nickel reaction path and the oxygen reaction path is very important in determining the charge efficiency of the cell. Only current flowing through the nickel reaction path leads to the effective accumulation of chemical energy inside the cell, whereas current flowing through the oxygen reaction path leads to pressure buildup and eventually to energy loss in the form of heat dissipation. The charge efficiency is highly influenced by both the value of the charge current and the cell temperature. For higher charge currents, the diffusion of H^{+} ions becomes a limiting factor of increasing importance for the rate of the nickel reaction. This means that the apparent nickel equilibrium potential $V^{eq\prime}_{Ni}$ will start to rise earlier in the charging process because of a larger value of the diffusion overpotential η_d, leading to an oxygen pressure buildup and hence a lower charge efficiency. For higher temperatures, the ratio between the rates of the nickel and oxygen reactions becomes smaller. This is caused by a difference in temperature dependence of the rates of both reactions. Fig. 6 shows the simulated partial currents flowing through the nickel and oxygen reaction paths in the nickel electrode during charging with a constant current of 100 mA at ambient temperatures of 0 and 60°C as a function of the SoC. The sum of both partial currents equals the charge current. At the higher temperature of 60°C, the oxygen reaction can be seen to take over a lot earlier in the charging process, leading to a poorer charge efficiency at higher temperatures. This is indeed found in experiments.

When batteries are not used for some time, they will loose stored energy by self-discharge, especially at higher temperatures. The phenomenon of self-discharge can easily be understood from the cell model in Fig. 3, with no externally applied load. Because the value of V^{o}_{Ni} is larger than $V^{o}_{O_2}$ (see Section 2), V^{eq}_{Ni} is higher than $V^{eq}_{O_2}$. Therefore, a loop current will flow counterclockwise through the parallel combination of the nickel and oxygen path in the nickel electrode. This leads to a decrease in stored energy at the nickel electrode and an increase in the amount of oxygen. The produced oxygen is reduced at the cadmium electrode, leading to a decrease in stored energy at the cadmium electrode through a similar loop current. Fig. 7 shows the simulated SoC at different ambient temperatures. At 25°C, about 80% of charge is lost after 75 days. This corresponds well to the typical average self-discharge rate reported in literature of about 1% a day at 25°C [29]. At higher temperatures, the rates of all electrochemical reactions become higher and consequently, the loop currents in the nickel and cadmium electrodes become higher, leading to a higher self-discharge rate, which agrees with the simulation results of Fig. 7.

Fig. 8 shows the simulated voltage, oxygen pressure and temperature curves during discharging and overdischarging at 25°C with a 600 mA discharging current. In the voltage curve, after approximately 1 h, a 0 V region

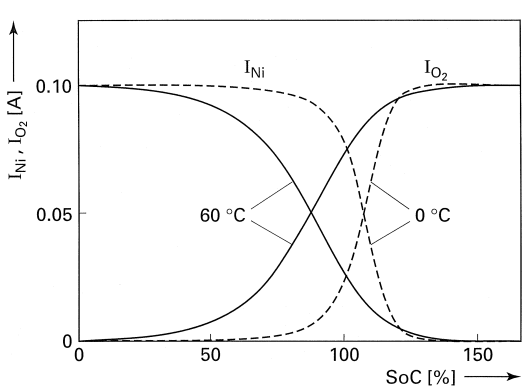

Fig. 6. Simulated partial nickel (I_{Ni}) and oxygen (I_{O_2}) currents as a function of State-of-Charge (SoC) in the nickel electrode during charging with a current of 100 mA at 0 and 60°C ambient temperature for an AA size 600 mAh rechargeable NiCd cell.

can be clearly recognized, followed by a region where the cell voltage is reversed. In this latter region, both the temperature and pressure increase and level off to a steady-state value. The phenomenon of overdischarging can be understood from the cell model given in Fig. 3.

The current direction in Fig. 3a is from right to left during discharging. During normal discharging, where the cell voltage remains at a relatively constant level of 1.3 V on the average, current will flow through the cadmium reaction path at the cadmium electrode and the nickel reaction path at the nickel electrode and the cell is effectively discharged. In the cadmium electrode, the amount of Cd decreases and the amount of $Cd(OH)_2$ increases. In the nickel electrode, the amount of NiOOH decreases and the amount of $Ni(OH)_2$ increases. As explained in Section 2, because of the excess amount of Cd at the cadmium electrode, the nickel electrode will run out of NiOOH before all Cd has been consumed at the cadmium electrode. Consequently, at the end of discharging, the exchange current I^{o}_{Ni} of the nickel reaction becomes low leading to a larger overpotential η_{Ni}, and the value of the apparent equilibrium potential $V^{eq\prime}_{Ni}$ becomes low, mainly because diffusion limitation of H^+ ions leads to a large value of the diffusion overpotential η_d. The current can no longer flow through the nickel reaction path. Besides, no current can flow through the oxygen reaction path, because there is no oxygen available yet to be reduced. Therefore, the current is forced to flow through the cadmium reaction path at the nickel electrode. Because identical reactions now occur at both electrodes, all current flows through both Cd reaction paths and the resulting cell voltage becomes close to 0 V.

When the amount of excess Cd at the cadmium electrode decreases to zero, the current starts to flow through the oxygen reaction path at the cadmium electrode. As a result, the amount of oxygen and hence the oxygen pressure will increase. Because of the difference in sign of V^{o} between the cadmium and the oxygen reaction, the potential of the cadmium electrode will now reverse. At the nickel electrode, the oxygen reduction starts to compete with the cadmium reaction. The reverse situation as described for the charging process now occurs. The cadmium electrode acts as a positive, oxygen forming electrode, whereas the nickel electrode acts as a negative electrode, where oxygen is reduced. As a result, the oxygen pressure will level off, as can be seen in Fig. 8. Again, because of the high overpotential of the oxygen reduction, now occurring at the nickel electrode, this reaction in particular produces a lot of heat, leading to a significant increase in temperature. The situation of cell voltage reversal can occur when cells are connected in series, as will be explained in the Section 5.

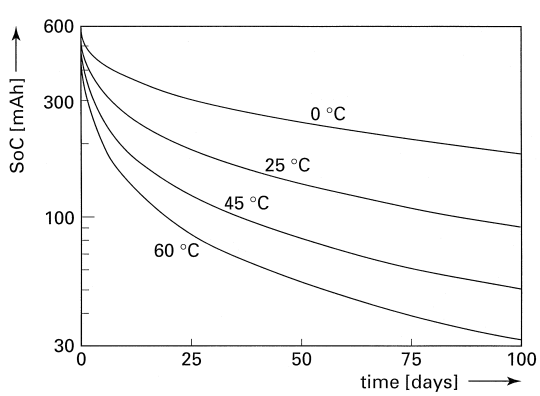

Fig. 7. Simulated State-of-Charge (SoC) as a function of time at different ambient temperatures for an AA size 600 mAh rechargeable NiCd cell.

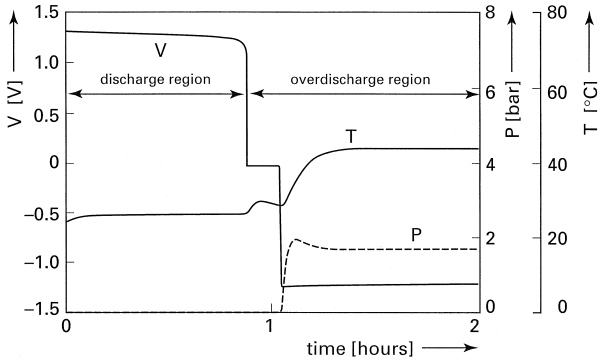

Fig. 8. Simulated voltage (V), oxygen pressure (P) and temperature (T) curves as a function of time during discharging and overdischarging at 25°C with a current of 600 mA for an AA size 600 mAh rechargeable NiCd cell.

5. Application of the NiCd cell model

Two examples are given in this section of using the cell model, in order to predict the negative effect of certain battery phenomena in an application. Based on these predictions, the design of the application could be altered in order to make optimal use of the battery. In the first example, the simulation result of a battery pack shows a possible reason for the often occurring breakdown of battery packs.

Series or parallel connections of cells in battery packs are often applied in practice in order to obtain a higher input voltage or a higher battery capacity. Fig. 9 shows the simulated battery pack voltage and oxygen pressure of one of its cells as a function of charge drawn from the battery (Q_{out}) during discharging at an ambient temperature of 25°C with a current of 600 mA. The battery pack was constructed by placing six cells in series. Two cases have been simulated. In case (a), all six cells inside the pack were given a capacity of 600 mAh. In case (b), all cells were given different capacities, ranging from 700 to 450 mAh in steps of 50 mAh to reflect spread in cell capacity, which depends on the type, manufacturer, usage history and age of the pack. The heat resistances between the six cells and between the cells and the environment were

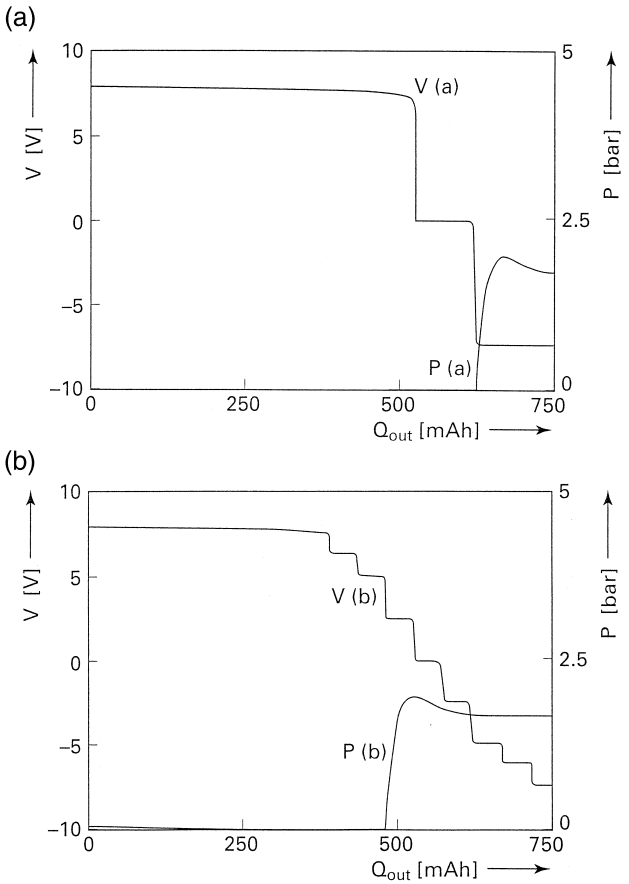

Fig. 9. Simulated voltage (V) and oxygen pressure (P) curves as a function of charge drawn from the battery (Q_{out}) during discharging with a current of 600 mA at 25°C. In (a), all six cells in the battery pack have a capacity of 600 mAh, in (b), the six cells display capacity spread from 700 to 450 mAh in steps of 50 mAh.

taken as zero for simplicity. In more advanced simulations, thermal models of the heat flows between the cells in a pack or from individual cells to the environment can be considered as well.

The curves for case (a) in Fig. 9 are basically the same as the voltage and pressure curves in Fig. 8. Because all cells have exactly the same capacity, all cells will be empty at exactly the same moment and the voltage curve is simply the sum of six identical voltage curves. The pressure curve (P(a)) shown is for only one cell, but it is the same for all six cells. The rise in oxygen pressure occurs when all the cells have reversed their voltages, as in Fig. 8. In practice, the pressure buildup will not take place in the case of identical cell capacities, because when the battery pack voltage decreases and approaches 0 V, the application does not operate anymore and discharging the pack will stop.

The curves for case (b) in Fig. 9 clearly show the result of the different capacities inside the battery pack. Curve V(b) shows the total pack voltage, whereas curve P(b) shows the pressure buildup inside the cell with the lowest capacity. The cell with the lowest capacity will be the first fully discharged cell and its voltage will become close to 0 V. This can be seen in curve V(b) as the first drop in battery pack voltage. Because the other cells still have a voltage of around 1.3 V, the battery pack voltage is still high enough to power the application and discharging is continued. Subsequently, the cell with the second lowest capacity reaches a voltage of approximately 0 V, which can be seen as the second drop in battery pack voltage. The third drop in battery pack voltage is due to voltage reversal of the cell with the lowest capacity. As a consequence, the oxygen pressure inside this cell will increase, as can be seen from curve P(b). The battery pack voltage

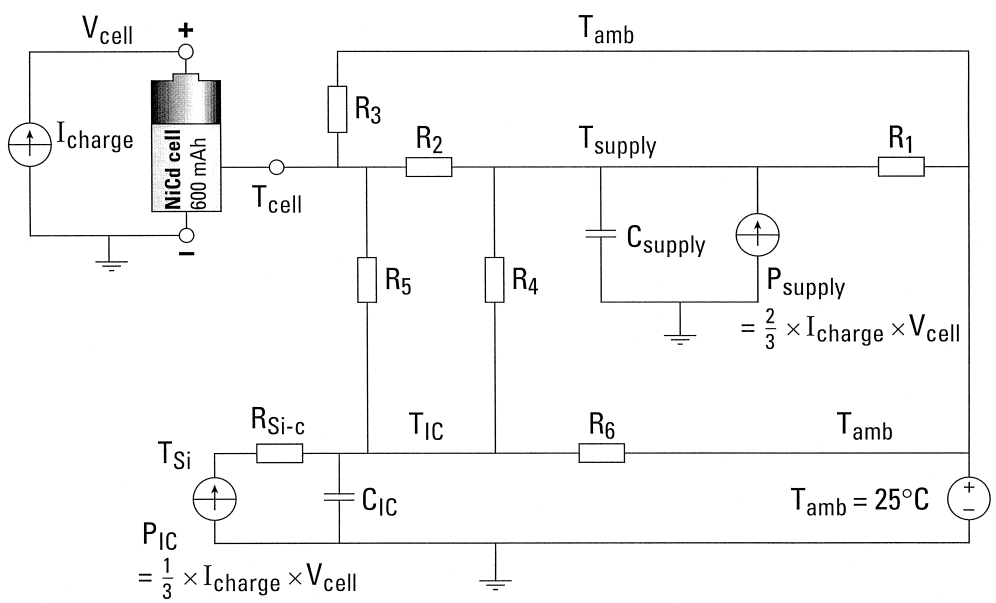

Fig. 10. Thermal and electrical simulation model of a shaver with integrated NiCd cell and charger (see also Table 3).

Table 3
Values of components in Fig. 10

Component	Description	Value	Unit
R_1	Heat resistance from remaining supply parts to ambient	47.2	K/W
R_2	Heat resistance from cell to remaining supply parts	93.3	K/W
R_3	Heat resistance from cell to ambient	40.8	K/W
R_4	Heat resistance from remaining supply parts to IC	49.8	K/W
R_5	Heat resistance from cell to IC	166	K/W
R_6	Heat resistance from IC to ambient	232	K/W
R_{Si-c}	Heat resistance from internal silicon to outside casing of IC	15	K/W
C_{IC}	Heat capacitance of IC	1.8	J/K
C_{supply}	Heat capacitance of remaining supply parts	8.4	J/K

at this moment is still around 2.5 V, which might allow discharging to be continued even further. High pressure buildup inside the cells may eventually lead to venting and loss of electrolyte, which degrades their performance. The simulation clearly shows that the battery pack is as strong as its weakest cell. Therefore, the capacities of cells inside a battery pack should match as closely as possible and the application should be shut off at an appropriate voltage level. The choice of this voltage level is a compromise between run time of the application and life time of the battery pack. The example clearly shows the need for a Battery Management System.

In some portable products, such as a shaver, the battery and charging electronics are packed close together inside the product. In the second example, charging a NiCd cell inside a shaver is simulated and a possible improved method of charging yielding better charge efficiency is presented. For the shaver for which simulations were performed, the charger inside is a Switched-Mode-Power Supply (SMPS) in flyback configuration [33], consisting of a rectifying mains buffer, transformer, charge–current regulation integrated circuit (IC) including the high voltage switch, rectifying secondary diode, and electrolytic smoothing output capacitor. Based on temperature difference and relaxation measurements of the chosen shaver, a simplified thermal model can be made with three heat producing components: the NiCd cell, the charge–current regulation IC and the remaining charger parts (transformer, rectifying mains buffer, diode). This thermal model can be coupled to the thermal network of the NiCd cell model at node T_{cell} shown in Fig. 3b, where the thermal network replaces R_{th} and C_{amb}. This is shown in Fig. 10, where the remaining charger parts are denoted as *supply*. Each heat producing component is coupled to the constant ambient temperature modelled by voltage source T_{amb} and to the two other heat producing components by means of heat resistances.

Each heat-producing component is modelled as a heat flow source, which models the dissipation, and a heat capacitance. For the IC, an extra heat resistance R_{Si-c} is shown, modelling the heat resistance from the integrated circuit in silicon to the outside casing. From practice, an efficiency of the power supply of 50% was found. Hence, a total power of $I_{charge}V_{cell}$ is dissipated in the power supply, of which approximately $1/3$ is dissipated in the IC and $2/3$ is dissipated in the remaining supply parts. The voltage at node T_{amb} denotes the constant ambient temperature, the voltage at node T_{IC} the IC casing temperature, the voltage at node T_{supply} the temperature of the remaining charger parts and the voltage at node T_{cell} the cell temperature. The values of the components in the thermal network model of Fig. 10, as deduced from measurements, are summarized in Table 3.

In Fig. 11, the simulated charge current, charge efficiency, SoC and cell temperature are shown as a function of time for the charging process of a rechargeable NiCd cell inside a shaver using the thermal network model shown in Fig. 10. The charge efficiency is defined as the ratio between effectively stored chemical energy and applied electrical energy. A constant charge current I_{charge} of 1.2 A was applied during 45 min. As can be seen from Fig. 11, the cell temperature rises to a value of around 60°C at the end of the charging process. The charge efficiency clearly drops at the end of charging, which is caused by the elevated temperature, as was also shown in Fig. 6. Moreover, the self-discharge rate becomes higher at elevated temperatures, as was shown in Fig. 7. As a result, with the current model parameter set the SoC of the cell drops at the end of charging, because the self-discharge

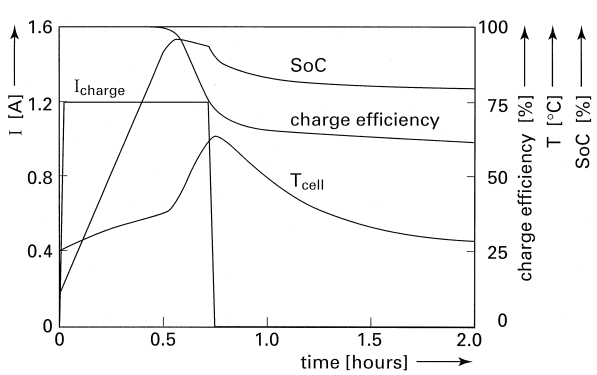

Fig. 11. Simulated charge current (I_{charge}), State-of-Charge (SoC), charge efficiency and cell temperature (T_{cell}) as a function of time for a charging process of an AA size 600 mAh rechargeable NiCd cell with a constant current of 1.2 A at 25°C inside a shaver.

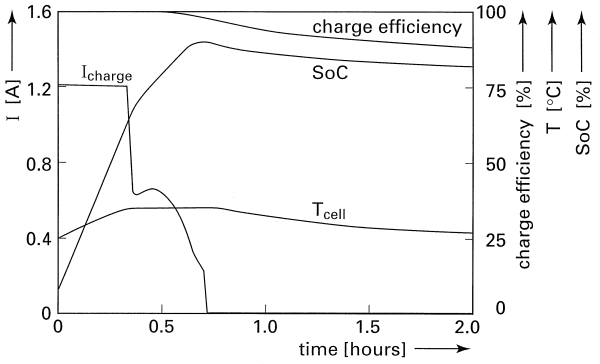

Fig. 12. Simulated charge current (I_{charge}), State-of-Charge (SoC), charge efficiency and cell temperature (T_{cell}) as a function of time for a thermostatic charging process of a 600 mAh rechargeable NiCd cell with a current starting at 1.2 A at 25°C inside a shaver. The cell temperature is not allowed to rise above 35°C.

rate becomes even higher than the rate at which energy is stored. After the current is interrupted, the rather high self-discharge rate leads to a continuing decrease in SoC and charge efficiency. In practice, the problem of reduced charge buildup inside small portable equipment with built-in charger, caused by too much heat evolution in a small volume and hence high temperatures, is commonly known.

An example of simulating the shaver, including the NiCd cell, to come up with an improved charging algorithm is shown in Fig. 12. All simulation conditions were chosen the same as in Fig. 11, except that the charge current I_{charge} was made a function of the cell temperature in such a way that the cell temperature never exceeds 35°C. This may be called *thermostatic* charging, i.e., charging with a maximum temperature, as opposed to *galvanostatic* charging with a fixed current. The total charge time was again chosen to be 45 min, as was the case for the galvanostatic simulation of Fig. 11. As can be seen from Fig. 12, the maximum cell temperature is 35°C by adapting the charge current I_{charge}. Due to the lower cell temperature, the drop in charge efficiency during charging is considerably less than in Fig. 11. Also, the drop in SoC is less than in Fig. 11. As a result, the charge efficiency increases from 62% for Fig. 11 to 87% for Fig. 12, leading to at least the same SoC after 2 h, although less electrical energy was supplied. A second advantage of thermostatic charging is that a longer cycle life of the cell due to a reduction in maximum temperature of the cell may be anticipated.

6. Conclusions

The construction and application of a simulation model for a sealed rechargeable NiCd cell was described in this paper. The simulation results presented in this paper show good qualitative agreement with measurements. Research is continued in order to find proper values for all parameters in the model to improve on quantitative agreement. Because the model already predicts important battery phenomena in a qualitative way, such as charge efficiency, self-discharge, overcharge and overdischarge behaviour, it can already be applied in the simulation of portable electronic systems to predict possible problems. Two examples of applying the model for such cases have been presented. For battery packs, a possible mechanism of breakdown and ways to prevent it have been described. By means of simulation of the charging process of a shaver, using a thermal model of the shaver, an alternative charging method yielding a better charge efficiency has been presented. Solutions for problems found during simulations can be implemented in the form of improved Battery Management Systems.

Although the approach is applied to rechargeable NiCd cells in this paper, it can also be applied to other rechargeable battery types, e.g., NiMH or Li-ion rechargeable batteries [34] and non-rechargeable batteries. Not all processes occurring in batteries have been included in the model at this moment. For example, ageing effects, which lead to the gradual loss of battery capacity when the battery becomes older, have not been included, because a good physical or chemical description of the ageing process lacks at the moment. Moreover, the memory effect, causing a reversible capacity loss when the battery is repeatedly partially charged and discharged, has not been included. However, when the corresponding mathematical equations behind these processes are found, they can readily be included in the model.

Acknowledgements

The authors would like to thank Siep Onneweer and Bram van den Akker for solving numerical problems occurring during the simulations. Rene van Beek is acknowledged for supplying the measured battery curves, Jan Reinder de Boer for supplying the thermal model of the shaver and Peter Blanken for fruitful discussions.

References

[1] J.J.L.M. van Vlerken, P.G. Blanken, Lumped modelling of rotary transformers, heads and electronics for helical-scan recording, IEEE Trans. Magn. 31 (2) (1995) 1050–1055.

[2] K.W. Choi, N.P. Yao, A mathematical model of porous nickel electrodes in zinc/nickel cells, in: S. Gross (Ed.), Battery Design and Optimisation, PV79-1, Electrochemical Society Proceedings Series, Princeton, NJ, 1979, pp. 62–80.

[3] K. Micka, I. Rousar, Theory of porous electrodes: XVI. The nickel hydroxide electrode, Electrochim. Acta 25 (1980) 1085–1090.

[4] K. Micka, I. Rousar, Theory of porous electrodes: XVII. Correction for anodic and cathodic reaction rates for nickel hydroxide electrodes, Electrochim. Acta 27 (1982) 765–769.

[5] J. Bouet, F. Richard, P. Blanchard, A discharge model for the Ni hydroxide positive electrode, in: D.A. Corrigan, A.H. Zimmerman (Ed.), Nickel Hydroxide Electrodes, PV 90-4, The Electrochemical Society Proceedings Series, Pennington, NJ, 1990, pp. 260–280.
[6] J.W. Weidner, P. Timmerman, Effect of proton diffusion, electron conductivity and charge-transfer resistance on nickel hydroxide discharge curves, J. Electrochem. Soc. 141 (2) (1994) 346–351.
[7] D. Fan, R.E. White, A mathematical model of a sealed nickel–cadmium battery, J. Electrochem. Soc. 138 (1) (1991) 17–25.
[8] D. Fan, R.E. White, Mathematical modelling of a nickel–cadmium battery—effects of intercalation and oxygen reactions, J. Electrochem. Soc. 138 (10) (1991) 2952–2960.
[9] Z. Mao, P. Vidts, R.E. White, Theoretical analysis of the discharge performance of a NiOOH/H_2 cell, J. Electrochem. Soc. 141 (1) (1994) 54–64.
[10] T.V. Nguyen, R.E. White, H. Gu, The effects of separator design on the discharge performance of a starved lead–acid cell, J. Electrochem. Soc. 137 (10) (1990) 2998–3004.
[11] M. Doyle, T.F. Fuller, J. Newman, Modelling of galvanostatic charge and discharge of the lithium/polymer/insertion cell, J. Electrochem. Soc. 140 (6) (1993) 1526–1533.
[12] T.F. Fuller, M. Doyle, J. Newman, Simulation and optimization of the dual lithium ion insertion cell, J. Electrochem. Soc. 141 (1) (1994) 1–10.
[13] E. Karden, P. Mauracher, F. Schöpe, Electrochemical modelling of lead/acid batteries under operating conditions of electric vehicles, J. Power Sources 64 (1) (1997) 175–180.
[14] S. Sathyanarayana, S. Venugopalan, M.L. Gopikanth, Impedance parameters and the State-of-Charge: I. Nickel–cadmium battery, J. Appl. Electrochem. 9 (1979) 125–139.
[15] N.A. Hampson, S.A.G.R. Karunathilaka, R. Leek, The impedance of electrical storage cells, J. Appl. Electrochem. 10 (1980) 3–11.
[16] A.H. Zimmerman, M.R. Martinelli, M.C. Janecki, C.C. Badcock, Impedance and mass transport kinetics of nickel cadmium cells, J. Electrochem. Soc. 129 (2) (1982) 289–293.
[17] S.A. Ilangovan, S. Sathyanarayana, Impedance parameters of individual electrodes and internal resistance of sealed batteries by a new nondestructive technique, J. Appl. Electrochem. 22 (1992) 456–463.
[18] S.C. Hageman, Simple PSpice Models Let You Simulate Common Battery Types, EDN, pp. 117–132, October 28, 1993.
[19] S.C. Hageman, PSpice Models Nickel–Metal–Hydride Cells, EDN, p. 99, February 2, 1995.
[20] S. Waaben, I. Moskowitz, J. Frederico, C.K. Dyer, Computer modelling of batteries from nonlinear circuit elements, J. Electrochem. Soc. 132 (6) (1985) 1356–1362.
[21] P.H.L. Notten, W.S. Kruijt, H.J. Bergveld, Electronic Network Modelling of Rechargeable Batteries, Ext. Abstract I-5-05, 46th ISE Meeting, Xiamen, China, 1995.
[22] P.H.L. Notten, W.S. Kruijt, H.J. Bergveld, Electronic Network Modelling of Rechargeable Batteries, Ext. Abstract 96, 191st ECS Meeting, Montreal, Canada, 1997.
[23] W.S. Kruijt, H.J. Bergveld, P.H.L. Notten, Electronic network modelling of rechargeable batteries: Part I. The nickel and cadmium electrodes, J. Electrochem. Soc. 145 (11) (1998) 3764–3773.
[24] P.H.L. Notten, W.S. Kruijt, H.J. Bergveld, Electronic network modelling of rechargeable batteries: Part II. The NiCd system, J. Electrochem. Soc. 145 (11) (1998) 3774–3783.
[25] W. Randszus, H.A. Kiehne (Eds.), Gasdichte Nickel–Cadmium Akkumulatoren, Varta Batterie, Hannover, Germany, 1978.
[26] S.G. Bratsch, Standard electrode potentials and temperature coefficients in water at 298.15 K, J. Phys. Ref. Data 18 (1) (1989) 1–21.
[27] R.C. Rosenberg, D.C. Karnopp, Introduction to Physical System Dynamics, McGraw-Hill, New York, 1983.
[28] J. Mc. Breen, The nickel oxide electrode, Mod. Asp. Electrochem. 21 (1990) 29–63.
[29] D. Linden, Handbook of Batteries, 2nd edn., McGraw-Hill, New York, 1995, pp. 28.13-28.15.
[30] J.S. Newman, Electrochemical Systems, 2nd edn., Prentice-Hall, Englewood Cliffs, NJ, 1991.
[31] A.J. Bard, L.R. Faulkner, Electrochemical Methods: Fundamentals and Applications, Wiley, New York, 1980.
[32] C.H. Hamann, W. Vielstich, Electrochemie II, Verlag Chemie, Weinheim, 1981.
[33] K.K. Sum, M.O. Thurston, Switch Mode Power Conversion; Basic Theory and Design, Electrical Engineering and Electronics, Vol. 22, Marcel Dekker, New York, 1984.
[34] W.S. Kruijt, E. de Beer, P.H.L. Notten, H.J. Bergveld, Electronic-Network Modelling of Rechargeable Li-based Battery Systems, Abstract 104, p. 114, The Electrochemical Society Meeting Abstracts, Vol. 97-2, Paris, France, Aug. 31–Sept. 5, 1997.